

Ultrafast optically induced spin transfer in ferromagnetic alloys

M. Hofherr, S. Häuser, J. K. Dewhurst, P. Tengdin, S. Sakshath, H. T. Nembach, S. T. Weber, J. M. Shaw, T. J. Silva, H. C. Kapteyn, M. Cinchetti, B. Rethfeld, M. M. Murnane, D. Steil, Benjamin Stadtmüller, S. Sharma, M. Aeschlimann, S. Mathias

Angaben zur Veröffentlichung / Publication details:

Hofherr, M., S. Häuser, J. K. Dewhurst, P. Tengdin, S. Sakshath, H. T. Nembach, S. T. Weber, et al. 2020. "Ultrafast optically induced spin transfer in ferromagnetic alloys." *Science Advances* 6 (3): eaay8717.
<https://doi.org/10.1126/sciadv.aay8717>.

PHYSICS

Ultrafast optically induced spin transfer in ferromagnetic alloys

M. Hoffherr^{1,2}, S. Häuser¹, J. K. Dewhurst³, P. Tengdin⁴, S. Sakshath¹, H. T. Nembach^{4,5}, S. T. Weber¹, J. M. Shaw⁵, T. J. Silva⁵, H. C. Kapteyn⁴, M. Cinchetti⁶, B. Rethfeld¹, M. M. Murnane⁴, D. Steil⁷, B. Stadtmüller^{1,2}, S. Sharma⁸, M. Aeschlimann¹, S. Mathias^{7*}

The vision of using light to manipulate electronic and spin excitations in materials on their fundamental time and length scales requires new approaches in experiment and theory to observe and understand these excitations. The ultimate speed limit for all-optical manipulation requires control schemes for which the electronic or magnetic subsystems of the materials are coherently manipulated on the time scale of the laser excitation pulse. In our work, we provide experimental evidence of such a direct, ultrafast, and coherent spin transfer between two magnetic subsystems of an alloy of Fe and Ni. Our experimental findings are fully supported by time-dependent density functional theory simulations and, hence, suggest the possibility of coherently controlling spin dynamics on subfemtosecond time scales, i.e., the birth of the research area of attomagnetism.

INTRODUCTION

Next-generation quantum materials will make it possible to surpass the speed and efficiency limits of current devices to generate faster, smaller, and more energy-efficient technological implementations (1–8). A promising approach to enhance data processing speed is to use ever shorter external stimuli for the manipulation and control of the state of matter. In this context, light represents the fastest means to alter the state of a material since laser pulses can now be generated with extremely short temporal duration down to a few tens of attoseconds. Visible lasers can deliver pulses with few-femtosecond durations that can be used to excite matter, while attosecond pulses can be generated in the extreme ultraviolet (EUV) and soft x-ray regions to probe the resulting dynamics (9–12). When combined with advanced spectroscopies, these new light sources are enabling comprehensive views into the fastest light-induced charge and spin dynamics in materials, on femtosecond to attosecond time scales. However, we are still far from understanding the basic light-matter interaction process itself that could, in principle, be used to directly manipulate the state of a material, particularly in strongly coupled systems (13–15).

Within a wide class of strongly coupled materials, magnetic systems are especially appealing from a technological point of view because new ultrafast control schemes have the potential to pave the way toward next-generation devices that can surpass the gigahertz operation speed of current devices. This quest toward ultrafast spintronics has simultaneously unearthed highly intriguing fundamental phenomena such as ultrafast demagnetization on femtosecond time scales (16) or the helicity-dependent all-optical switching of magnetic materials (17). Most work to date assumed that laser excitation of a magnetic

material results in a nonequilibrium hot charge distribution, which subsequently triggers a series of cascaded incoherent secondary processes including transport, (spin-flip) scattering, and quasiparticle generation, ultimately leading to macroscopic demagnetization of the magnetic material within <500 fs (18–22).

The fastest manipulation of the magnetic state should occur, however, through the direct (possibly coherent) interaction between the spin system of the material and the light field itself (23–25). While the first experiments have provided indications that such a direct manipulation scheme might be possible (26–29), to our knowledge, only one experimental study on magnetic metallic systems to date has focused on this challenging aspect of coherent ultrafast magnetism induced by femtosecond laser pulses (24). One particularly interesting and previously unknown scheme for the ultrafast manipulation of spins using light takes advantage of the optically induced spin transfer (OISTR) effect, which was recently introduced by Dewhurst *et al.* (30). In their theoretical work, it was shown that optical excitation can directly, coherently, and efficiently redistribute spins between different magnetic sublattices in a multicomponent magnetic material. Crucially, this process does not alter the total magnetization of the material, but rather redistributes the spins between the different magnetic subsystems, which makes this effect particularly attractive from a fundamental as well as an application-oriented point of view. It is, therefore, important to experimentally test whether coherent interactions on the time scale of the optical excitation, such as the OISTR effect, can indeed induce a sizeable modification of the magnetic state in functional materials. This opens a previously unknown avenue toward manipulating solids on time scales only limited by the duration of the exciting light pulse, which is substantially shorter than the usually discussed ultrafast but incoherent spin dynamics [for a review, see (21)] that evolve after the optical excitation.

RESULTS

In this work, we therefore investigate the experimental fingerprint of such a coherent spin transfer process in an Fe₅₀Ni₅₀ alloy. We show that the Fe₅₀Ni₅₀ alloy has a band structure and density of states that enable efficient light-driven coherent spin transfer from the Ni to the Fe magnetic subsystem (see Fig. 1, A and B), i.e., it enables the

Copyright © 2020
The Authors, some
rights reserved;
exclusive licensee
American Association
for the Advancement
of Science. No claim to
original U.S. Government
Works. Distributed
under a Creative
Commons Attribution
NonCommercial
License 4.0 (CC BY-NC).

Downloaded from <https://www.science.org at Universitaetsbibliothek Augsburg on May 14, 2024>

¹Technische Universität Kaiserslautern und Landesforschungszentrum OPTIMAS, Erwin-Schroedinger Strasse 46, 67663 Kaiserslautern, Germany. ²Graduate School of Excellence Materials Science in Mainz, Staudinger Weg 9, 55128 Mainz, Germany. ³Max Planck Institute of Microstructure Physics, Weinberg 2, 06120 Halle, Germany. ⁴Department of Physics and JILA, University of Colorado and NIST, Boulder, CO 80309, USA. ⁵Quantum Electromagnetics Division, National Institute of Standards and Technology, Boulder, CO 80305, USA. ⁶Experimentelle Physik VI, Technische Universität Dortmund, 44221 Dortmund, Germany. ⁷Georg-August-Universität Göttingen, I. Physikalisches Institut, Friedrich-Hund-Platz 1, 37077 Göttingen, Germany. ⁸Max Born Institute for Nonlinear Optics, Max-Born-Strasse 2A, 12489 Berlin, Germany.

*Corresponding author. Email: smathias@uni-goettingen.de

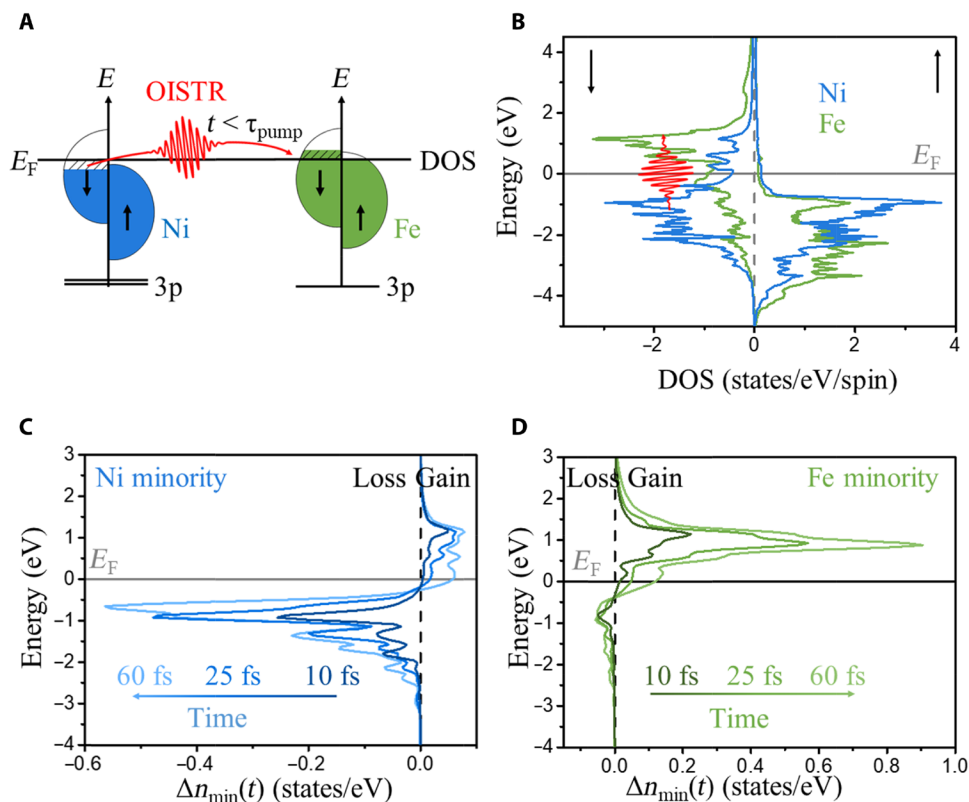


Fig. 1. Ultrafast OISTR in $\text{Fe}_{50}\text{Ni}_{50}$. (A) Schematic overview of the OISTR effect in $\text{Fe}_{50}\text{Ni}_{50}$. The optical excitation by the IR pump leads to an effective spin transfer from the occupied Ni minority channel into the Fe minority channel. Note that other excitations are also possible, and significant OISTR can only be expected if such a spin transfer transition dominates the full excitation process. (B) Projected density of states (DOS) calculation for $\text{Fe}_{50}\text{Ni}_{50}$ for Fe (green) and Ni (blue) demonstrating the favorable spin transfer from Ni to Fe in the minority channel. (C and D) TD-DFT calculations of the difference of the transient occupation compared with the unexcited case in the minority channels of Ni (C) and Fe (D) at characteristic time steps demonstrating the OISTR effect. In Ni at energies between 0.5 and 3 eV below the Fermi level, a negative signal arises corresponding to a loss of minority electrons, while a simultaneous positive signal correlating to minority spin gain is visible in Fe at equivalent energies above the Fermi level.

observation of the OISTR process. The OISTR mechanism for the $\text{Fe}_{50}\text{Ni}_{50}$ alloy is illustrated in Fig. 1A. An optical excitation directly transfers spin carriers between the magnetic subsystems on the time scale of the ultrashort infrared (IR) pump pulse. This OISTR process is most efficient when the photon energy of the IR pulse coincides with a resonant transition between one spin channel in both elemental subsystems, and this transition is dominant in comparison to all other possible optical excitations in the material (not shown in the scheme). Only then, a significant spin transfer will take place between both subsystems, and hence, the OISTR effect can be expected. It is important to note that this spin transfer process generates a pure spin current, i.e., nearly no dipole moment is induced (30), which strongly contrasts the process from optical doping. For $\text{Fe}_{50}\text{Ni}_{50}$, pumping with IR light is expected to initiate spin transfer via a resonant interband excitation between minority bands of the $\text{Fe}_{50}\text{Ni}_{50}$ alloy. Guided by time-dependent density functional theory (TD-DFT) calculations, we are able to monitor the optically induced transient changes in the population of the Fe- and Ni-dominated minority and majority bands in real time by time-resolved magneto-optical Kerr (MOKE) spectroscopy. To gain element specificity, we use a short-wavelength EUV high-harmonic light source (31), and we use the transversal MOKE geometry, which is sensitive to the in-plane magnetization of materials and allows us to monitor transient magnetization changes of both sublattices by recording intensity

changes of the reflected EUV light for two opposite magnetic fields (32–35).

We find that such a tailored binary material system indeed enables ultrafast, efficient, and coherent manipulation of the magnetic properties on the time scale of the ultrashort (30 ± 5 fs) pump pulse. The TD-DFT calculations further verify that our experimental findings are consistent with the theoretically predicted OISTR mechanism in magnetic materials (30). In this way, our observation lays the foundation for coherent control schemes on extremely short time scales down to the pulse width of the shortest light pulse generated so far.

To reveal the spectroscopic fingerprint of the OISTR effect, we first need to identify energy regions of the band structure of a particular material that are strongly affected by optically induced coherent spin transfer between magnetic subsystems. Guided by a previous work (34), where peculiar spin dynamics during the laser pulse were observed but were not discussed nor explained, we performed TD-DFT calculations for FeNi alloys. Being a fully ab initio method to describe light-matter interaction, TD-DFT has the advantage that the underlying physics of laser-induced spin dynamics is an emergent quantity and is not assumed. Moreover, the treatment is nonperturbative in the sense that it is not just a linear treatment but also all the higher-order effects are taken into account. To ensure numerical accuracy, all calculations were performed in two steps using a state-of-the-art full-potential linearized augmented plane wave (LAPW) technique

(36) as implemented in the Elk code (37): First, the ground state is determined using DFT. We have used an $L1_0$ crystal structure with fully optimized lattice parameters to simulate ordered FeNi alloys. This leads to corresponding ground-state moment on Fe and Ni atoms. Second, this ground state is then time propagated (36) under the influence of a pump laser pulse of 5 mJ/cm^2 , a full width at half maximum (FWHM) of 40 fs, and a photon energy of 1.55 eV. We intentionally used a theoretical pulse duration longer than the experimental pump duration to account for the measured cross-correlation with the probe pulse. During the time propagation, we monitor the atom-resolved transient occupations (38) at each time step (2 as).

Accordingly, Fig. 1 (C and D) shows the TD-DFT-derived spectrally resolved optically induced modifications (colored lines) in the occupation of the minority spin channels of Fe and Ni with respect to the unperturbed material (dashed vertical line at $\Delta n_{\text{min}} = 0$). Besides other excitations (not shown), the most notable transient change below the Fermi level occurs in the minority channel of Ni (Fig. 1C). Here, optical excitation leads to a significant reduction in the number of minority spin carriers as a function of time, which corresponds to an increase in the Ni sublattice magnetization. Note that because of the multiphoton photoexcitation processes, dynamics are present in an energy range larger than the pump laser pulse energy of 1.55 eV.

The calculations show that electrons are transferred from minority Ni states to minority Fe states by the ultrashort IR laser pulse. Consequently, we find a simultaneous accumulation of charge and spin carriers in the minority states of Fe above the Fermi level, also due to the optical excitation. We note that although changes in the occupation of the majority states also occur, these are much less pronounced and therefore will not be discussed further (see the Supplementary Materials). Thus, the TD-DFT calculations indicate that efficient ultrafast and coherent OISTR can be driven by a 30-fs duration laser pulse, with a photon energy in the IR regime centered at 1.55 eV, which predominantly transfers spin carriers from the occupied Ni minority to the unoccupied Fe minority states in an $\text{Fe}_{50}\text{Ni}_{50}$ alloy.

Guided by these theoretical predictions, we experimentally probed the magnetic dynamics in $\text{Fe}_{50}\text{Ni}_{50}$, taking advantage of the sensitivity of EUV transversal MOKE (TMOKE) measurements to the magnetic state of each individual element in the alloy (34). Figure 2A shows a schematic of the experiment. IR laser pump pulses with a repetition rate of 6 kHz, and an FWHM pulse duration of 30 fs are used to trigger the Ni and the Fe sublattices. EUV pulses with photon energies between 30 and 72 eV were generated via high-harmonic generation (HHG) by focusing laser pulses from the same laser into a neon-filled hollow waveguide. The reflected EUV intensities recorded for two opposite directions of the sample magnetization I_+ and I_- are used to calculate the magnetic asymmetry $A = \frac{I_+ - I_-}{I_+ + I_-}$, which is, in first-order approximation, proportional to the magnetization in the sample (39, 40). Figure 2B displays an example TMOKE asymmetry of the $\text{Fe}_{50}\text{Ni}_{50}$ alloy as a function of the photon energy in the vicinity of the Fe (left) and the Ni (right) $M_{2,3}$ absorption edges, extending over an energy interval of several electron volts in the EUV range (39–42).

In general, the magneto-optical response of a material provides a direct probe of the spin polarization of the occupied and unoccupied magnetic bands involved in the optical transitions available at a given wavelength (39, 43). Because the $M_{2,3}$ core levels are both energetically narrow and spin degenerate, the magnetic asymmetry is directly correlated to the element-resolved spin polarization in the vicinity of the Fermi level. However, to date, most femtosecond magneto-

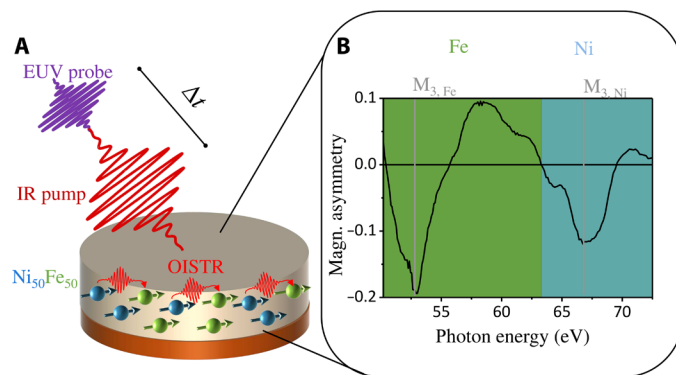


Fig. 2. Schematic of the conducted OISTR experiment. (A) Experimental setup. An EUV probe pulse investigates the element-specific magnetization dynamics in $\text{Fe}_{50}\text{Ni}_{50}$ triggered by an IR pump. (B) Magnetic asymmetry of Fe and Ni plotted as a function of the photon energy. The shaded green and blue energy ranges mark the energy range that is commonly integrated in an absorption edge experiment to obtain the total magnetization.

optical experiments at the M- (and L-) absorption edges have focused on the element-specific dynamics of the total magnetization (32–34, 44–47). This information is often extracted by integrating the magnetic asymmetry across the absorption edge of each element (shaded areas in Fig. 2B). In contrast, here we go beyond this approach by extracting the transient spin polarization in different regions of the valence band structure (48), in particular to observe the signature of the OISTR effect.

The TD-DFT calculations discussed above predict that the IR laser excitation should lead to an efficient spin transfer from the Ni minority to the Fe minority states. The spectroscopic fingerprints of the evolving coherent manipulation of the spin polarization should therefore appear in the corresponding spectral range of the Ni and Fe M-absorption edges. Energy-dependent changes in the MOKE asymmetry, hence, serve as an element-specific probe for optically induced modifications of the spin polarization of Ni and Fe. Accordingly, we performed a spectral analysis of our experimental time-resolved magnetic asymmetry data. We note that the high signal-to-noise ratio required for this analysis restricted us to energy regions with high peak intensities of the reflected EUV light (i.e., near the peaks of the odd harmonics of the driving laser; see the Supplementary Materials). To compare the experimental asymmetry data and the spin polarization dynamics in the vicinity of the Fermi level, Fig. 3A displays the asymmetry as a function of final-state energy of the EUV absorption signal, where the M_3 core level energies of 52.7 eV for Fe and 66.2 eV for Ni (49) were subtracted from the measured photon energy, respectively (see the Supplementary Materials).

Figure 3B displays the transient change of the experimental asymmetry, i.e., the experimental spin polarization, for states below the Fermi level in Ni (dark blue line) and for states above the Fermi level in Fe (dark green line). The Fe asymmetry is substantially reduced, while that of Ni increases, as might be expected if the OISTR effect is playing a role, inducing a depletion of minority spin carriers for Ni and a simultaneous accumulation of minority spins in Fe. The corresponding element-specific transient spin polarization predicted by our TD-DFT calculation is included as light blue and green solid lines, respectively. The data of Fig. 3B exhibit fast and mirrored dynamics on time scales of ≈ 50 fs, i.e., on the same time scale as the optical excitation.

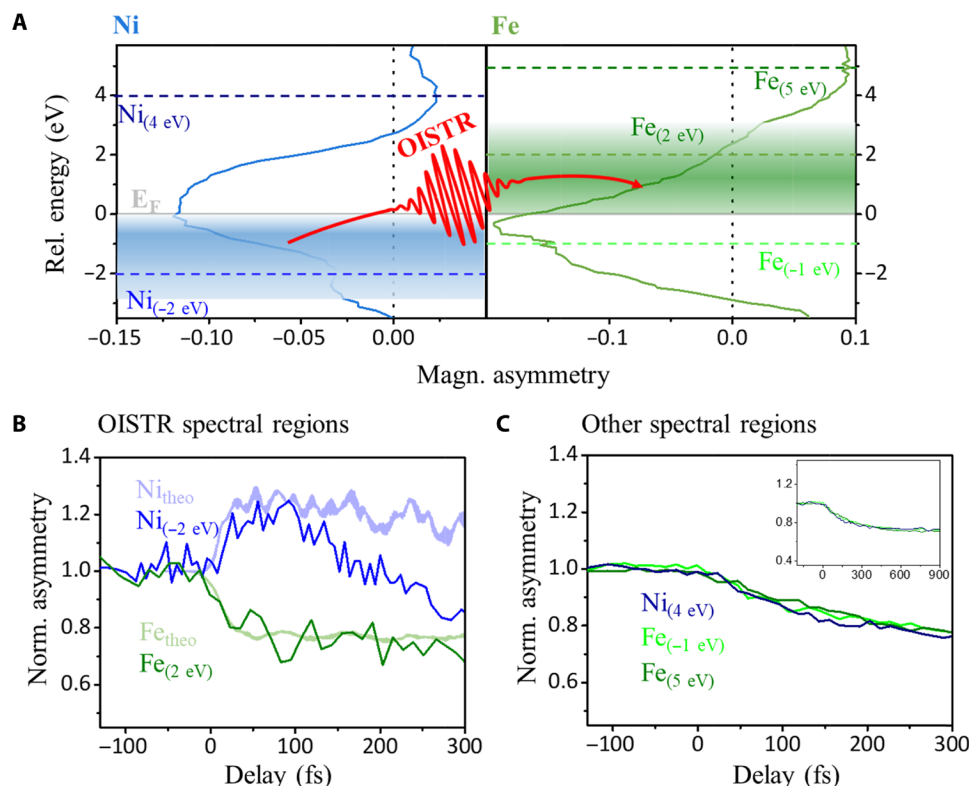


Fig. 3. Direct time-resolved verification of the OISTR effect on ultrashort time scales. (A) Static magnetic asymmetry of Fe and Ni plotted as a function of the energy relative to the Fermi level, i.e., the measured photon energy after subtracting the M_3 core level energy. (B and C) Spectral dynamics of the magnetic asymmetry of Fe and Ni for different spectral regions. (B) In the energy regions marked in (A) by the shaded colored bars according to the calculations shown in Fig. 1, the spin dynamics show a clear fingerprint of OISTR, on ~ 50 -fs time scales. (C) In contrast, other spectral regions display only the conventional demagnetization caused by multistep relaxation processes. The inset shows the demagnetization dynamics on a longer time scale, revealing a quenching level of $\sim 25\%$ to which all spectral regions converge. Note that the integrated signals averaging over extended spectral regions show the typical delayed behavior between Fe and Ni (see the Supplementary Materials), as seen before (34). The characteristic energies that are analyzed are marked in (A) with the dashed lines.

As a further cross-check for OISTR, Fig. 3C displays the time-dependent asymmetry traces for energy regions for which the contribution of the OISTR effect is expected to be absent. These energies are, for instance, above and below the Fermi level of Ni and Fe, respectively (blue and light green line), and far above the Fermi level of Fe (dark green line). We indeed extract the same demagnetization response of a strongly exchange-coupled alloy observed previously (34), with no indication of the OISTR effect at these energies, as expected from theory.

DISCUSSION

We now turn to a more detailed comparison between the theoretical and experimental data shown in Fig. 3B. First, we note that the strength of the spin transfer critically depends on the absorbed pump laser fluence, which is in the region of several mJ/cm^2 , but is hard to determine with higher accuracy for our particular setup. We, therefore, display in Fig. 3B theoretical data that have been adapted for an absorbed fluence of $5\text{ mJ}/\text{cm}^2$ to match the loss in spin polarization in the experimental Fe data. We observe that this adaption simultaneously results in a very good quantitative agreement with the observed experimental increase in the spin polarization in Ni. Crucially, we even find a quantitative agreement between the predicted and observed time-dependent magnetic dynamics—both experiment and

theory show identical element-resolved changes in the sublattice spin polarization up to 100 fs. Thereafter, the experimental Ni spin polarization decays mainly because of incoherent, secondary spin-flip and possibly following magnon generation processes, which are not included in the theoretical model. Notably, the OISTR dynamics evolve during the laser excitation, i.e., the optical transition itself, resulting in the fastest transfer of spins between the two magnetic subsystems.

In addition, as mentioned above, OISTR is not the only process that evolves during the time scale of the femtosecond optical excitation. For instance, it has just recently been shown that ultrafast spin excitations (28) and nonequilibrium spin polarizations (26, 27) also evolve on the time scale of the optical laser pulse itself (i.e., up to about 30 fs in our case). Although these processes could potentially contribute to the dynamics that we observe, the good agreement between our TD-DFT calculations and experimental findings strongly suggests that OISTR is the dominant process here. Furthermore, a comparison to $\text{Fe}_{20}\text{Ni}_{80}$ (not shown), which did show peculiar behavior in a previous study (34), indicates that an OISTR effect is also present in $\text{Fe}_{20}\text{Ni}_{80}$ but is much more pronounced for $\text{Fe}_{50}\text{Ni}_{50}$, the sample of choice for the present work.

Last, we would like to comment on the interpretation of the spin transfer in an alloy with a nearly itinerant band structure. When combining two transition metals in an alloy, the atomic orbitals begin to hybridize (50, 51) and start forming a joint delocalized band

structure. However, it is commonly accepted that in general, not all bands completely lose their atomic orbital character and hence retain partially their initial elemental character—as has been shown both experimentally (34, 52, 53) and theoretically (38, 50, 54). The amount of hybridization can be evaluated by calculating the projected density of states. Accordingly, within this framework, a spin transfer in Fe₅₀Ni₅₀ can be understood as a transition from a band with a predominant Ni character to an unoccupied band with a predominant Fe character.

In conclusion, we used time-resolved HHG TMOKE to directly observe a coherent net spin transfer between the two subsystems in Fe₅₀Ni₅₀ on the time scale of the optical excitation. By extracting the spectral information contained in the magnetic asymmetry data, we were able to unambiguously reveal a transient energy-dependent modification of the spin polarization in Fe and Ni consistent with a direct spin transfer from Ni to Fe. Our experimental observations can be described by the OISTR effect, resulting in a simultaneous increase in the Ni spin polarization below the Fermi level and a corresponding decrease in the spin polarization of the occupied Fe states. TD-DFT calculations fully support our experimental data matching both in the spectral dependence and in the observed femtosecond dynamics. We believe that our findings are of a very general nature and can be extended to a variety of magnetic heterostructures. Last, as an immediate consequence of the results obtained in this work, we forecast a control of the spin dynamics on the attosecond time scale, and note that a first light-wave dynamic control of magnetization has indeed recently been identified (55). This not only will allow us to explore the fundamental limits of material science and magnetism to ever smaller length and ever faster time scales, but will also have intriguing consequences for future information technology application. Coherent control of matter can potentially yield previously unknown concepts to substantially reduce the operation time of next-generation spintronic devices, down to the time duration of the shortest light pulse that can be generated.

MATERIALS AND METHODS

TD-DFT and computational details

The Runge-Gross theorem (56) establishes that the time-dependent external potential is a unique functional of the time-dependent density, given the initial state. On the basis of this theorem, a system of noninteracting particles can be chosen such that the density of this noninteracting system is equal to that of the interacting system for all times (57). The wave function of this noninteracting system is represented as a Slater determinant of single-particle orbitals. In what follows, a fully noncollinear spin-dependent version of these theorems is used (25). Then, the time-dependent Kohn-Sham (KS) orbitals are Pauli spinors determined by the equations

$$i \frac{\partial \psi_j(\mathbf{r}, t)}{\partial t} = \left[\frac{1}{2} \left(-i\nabla + \frac{1}{c} \mathbf{A}_{\text{ext}}(t) \right)^2 + v_s(\mathbf{r}, t) + \frac{1}{2c} \boldsymbol{\sigma} \cdot \mathbf{B}_s(\mathbf{r}, t) + \frac{1}{4c^2} \boldsymbol{\sigma} \cdot (\nabla_{v_s(\mathbf{r}, t)} \times -i\nabla) \right] \psi_j(\mathbf{r}, t) \quad (1)$$

where $\mathbf{A}_{\text{ext}}(t)$ is a vector potential representing the applied laser field and $\boldsymbol{\sigma}$ are the Pauli matrices. The KS effective potential $v_s(\mathbf{r}, t) = v_{\text{ext}}(\mathbf{r}, t) + v_{\text{H}}(\mathbf{r}, t) + v_{\text{xc}}(\mathbf{r}, t)$ is decomposed into the external potential v_{ext} , the classical electrostatic Hartree potential v_{H} , and the exchange-correlation (XC) potential v_{xc} . Similarly, the KS magnetic field is

written as $\mathbf{B}_s(\mathbf{r}, t) = \mathbf{B}_{\text{ext}}(t) + \mathbf{B}_{\text{xc}}(\mathbf{r}, t)$, where $\mathbf{B}_{\text{ext}}(t)$ is the magnetic field of the applied laser pulse and possibly an additional external magnetic field and $\mathbf{B}_{\text{xc}}(\mathbf{r}, t)$ is the XC magnetic field. The final term of Eq. 1 is the spin-orbit coupling term. It is assumed that the wavelength of the applied laser is much greater than the size of a unit cell, and the dipole approximation can be used, i.e., the spatial dependence of the vector potential is disregarded. For XC potential, adiabatic local spin density approximation was used (58).

All calculations used the state-of-the-art full potential LAPW method. Within this method, the core electrons (with eigenvalues 95 eV below Fermi energy) were treated fully relativistically by solving the radial Dirac equation, while higher-lying electrons were treated using the scalar relativistic Hamiltonian in the presence of the spin-orbit coupling. To obtain the two-component Pauli spinor states, the Hamiltonian containing only the scalar potential was diagonalized in the LAPW basis: This is the first variational step. The scalar states thus obtained were then used as a basis to set up a second variational Hamiltonian with spinor degrees of freedom (59). A fully noncollinear version of TD-DFT as implemented within the Elk code (37) was used for all calculations (60). A regular mesh in \mathbf{k} -space $8 \times 8 \times 8$ was used, and a time step of $\Delta t = 0.002$ fs was used for the time propagation algorithm (36). A smearing width of 0.027 eV was used. For all ground-state calculations, a full structural optimization was performed. We found that the effect of lattice relaxation were very small in spin dynamics in this material.

SUPPLEMENTARY MATERIALS

Supplementary material for this article is available at <http://advances.sciencemag.org/cgi/content/full/6/3/eaay8717/DC1>

Section S1. Spectrum

Section S2. Majority dynamics

Section S3. Two separated core levels for Ni

Section S4. Energy integrated signals

Fig. S1. High-harmonic spectrum reflected from the FeNi sample.

Fig. S2. Transient occupations in Fe and Ni majority channels.

Fig. S3. Schematic depiction on the influence of two separated core levels for Ni.

Fig. S4. Energy integrated magnetization dynamics for Fe and Ni in Fe₅₀Ni₅₀.

REFERENCES AND NOTES

- C.-H. Lambert, S. Mangin, B. S. D. Ch. S. Varaprasad, Y. K. Takahashi, M. Hehn, M. Cinchetti, G. Malinowski, K. Hono, Y. Fainman, M. Aeschlimann, E. E. Fullerton, All-optical control of ferromagnetic thin films and nanostructures. *Science* **345**, 1337–1340 (2014).
- M. N. Baibich, J. M. Broto, A. Fert, F. van Nguyen Dau, F. Petroff, P. Etienne, G. Creuzet, A. Friederich, J. Chazelas, Giant magnetoresistance of (001)Fe/(001)Cr magnetic superlattices. *Phys. Rev. Lett.* **61**, 2472–2475 (1988).
- G. Binasch, P. Grünberg, F. Saurenbach, W. Zinn, Enhanced magnetoresistance in layered magnetic structures with antiferromagnetic interlayer exchange. *Phys. Rev. B* **39**, 4828 (1989).
- S. A. Wolf, D. D. Awschalom, R. A. Buhrman, J. M. Daughton, S. von Molnár, M. L. Roukes, A. Y. Chtchelkanova, D. M. Treger, Spintronics: A spin-based electronics vision for the future. *Science* **294**, 1488–1495 (2001).
- A. V. Chumak, A. A. Serga, B. Hillebrands, Magnon transistor for all-magnon data processing. *Nat. Commun.* **5**, 4700 (2014).
- S. S. P. Parkin, M. Hayashi, L. Thomas, Magnetic domain-wall racetrack memory. *Science* **320**, 190–194 (2008).
- D. Atkinson, D. A. Allwood, G. Xiong, M. D. Cooke, C. C. Faulkner, R. P. Cowburn, Magnetic domain-wall dynamics in a submicrometre ferromagnetic structure. *Nat. Mater.* **2**, 85–87 (2003).
- I. Tudosa, C. Stamm, A. B. Kashuba, F. King, H. C. Siegmann, J. Stöhr, G. Ju, B. Lu, D. Weller, The ultimate speed of magnetic switching in granular recording media. *Nature* **428**, 831–833 (2004).
- G. Sansone, E. Benedetti, F. Calegari, C. Vozzi, L. Avaldi, R. Flammini, L. Poletto, P. Villoresi, C. Altucci, R. Velotta, S. Stagira, S. de Silvestri, M. Nisoli, Isolated single-cycle attosecond pulses. *Science* **314**, 443–446 (2006).

10. Y. Mairesse, A. de Bohan, L. J. Frasinski, H. Merdji, L. C. Dinu, P. Monchicourt, P. Breger, M. Kovacev, R. Taieb, B. Carre, H. G. Muller, P. Agostini, P. Salieres, Attosecond synchronization of high-harmonic soft x-rays. *Science* **302**, 1540–1543 (2003).
11. J. Li, X. Ren, Y. Yin, K. Zhao, A. Chew, Y. Cheng, E. Cunningham, Y. Wang, S. Hu, Y. Wu, M. Chini, Z. Chang, 53-attosecond X-ray pulses reach the carbon K-edge. *Nat. Commun.* **8**, 186 (2017).
12. I. P. Christov, M. M. Murnane, H. C. Kapteyn, High-Harmonic Generation of Attosecond Pulses in the “Single-Cycle” Regime. *Phys. Rev. Lett.* **78**, 1251 (1997).
13. L. Perfetti, P. A. Loukakos, M. Lisowski, U. Bovensiepen, H. Berger, S. Biermann, P. S. Cornaglia, A. Georges, M. Wolf, Time evolution of the electronic structure of 1T-TaS₂ through the insulator-metal transition. *Phys. Rev. Lett.* **97**, 67402 (2006).
14. T. Rohwer, S. Hellmann, M. Wiesenmayer, C. Sohr, A. Stange, B. Slomski, A. Carr, Y. Liu, L. M. Avila, M. Kallane, S. Mathias, L. Kipp, K. Rossnagel, M. Bauer, Collapse of long-range charge order tracked by time-resolved photoemission at high momenta. *Nature* **471**, 490–493 (2011).
15. D. Fausti, R. I. Tobey, N. Dean, S. Kaiser, A. Dienst, M. C. Hoffmann, S. Pyon, T. Takayama, H. Takagi, A. Cavalleri, Light-induced superconductivity in a stripe-ordered cuprate. *Science* **331**, 189–191 (2011).
16. E. Beaurepaire, J.-C. Merle, A. Daunois, J.-Y. Bigot, Ultrafast spin dynamics in ferromagnetic nickel. *Phys. Rev. Lett.* **76**, 4250 (1996).
17. C. D. Stanciu, F. Hansteen, A. V. Kimel, A. Kirilyuk, A. Tsukamoto, A. Itoh, T. Rasing, All-optical magnetic recording with circularly polarized light. *Phys. Rev. Lett.* **99**, 47601 (2007).
18. M. Krauß, T. Roth, S. Alebrand, D. Steil, M. Cinchetti, M. Aeschlimann, H. C. Schneider, Ultrafast demagnetization of ferromagnetic transition metals: The role of the Coulomb interaction. *Phys. Rev. B* **80**, 180407 (2009).
19. M. Battiato, K. Carva, P. M. Oppeneer, Superdiffusive spin transport as a mechanism of ultrafast demagnetization. *Phys. Rev. Lett.* **105**, 27203 (2010).
20. B. Koopmans, G. Malinowski, F. Dalla Longa, D. Steiauf, M. Fähnle, T. Roth, M. Cinchetti, M. Aeschlimann, Explaining the paradoxical diversity of ultrafast laser-induced demagnetization. *Nat. Mater.* **9**, 259–265 (2010).
21. A. Kirilyuk, A. V. Kimel, T. Rasing, Ultrafast optical manipulation of magnetic order. *Rev. Mod. Phys.* **82**, 2731 (2010).
22. D. Hinzke, U. Atxitia, K. Carva, P. Nieves, O. Chubykalo-Fesenko, P. M. Oppeneer, U. Nowak, Multiscale modeling of ultrafast element-specific magnetization dynamics of ferromagnetic alloys. *Phys. Rev. B* **92**, 54412 (2015).
23. G. P. Zhang, W. Hübner, Laser-induced ultrafast demagnetization in ferromagnetic metals. *Phys. Rev. Lett.* **85**, 3025 (2000).
24. J.-Y. Bigot, M. Vohr, E. Beaurepaire, Coherent ultrafast magnetism induced by femtosecond laser pulses. *Nat. Phys.* **5**, 515–520 (2009).
25. K. Krieger, J. K. Dewhurst, P. Elliott, S. Sharma, E. K. U. Gross, Laser-induced demagnetization at ultrashort time scales: Predictions of TDDFT. *J. Chem. Theory Comput.* **11**, 4870–4874 (2015).
26. S. Eich, M. Plötzing, M. Rollinger, S. Emmerich, R. Adam, C. Chen, H. C. Kapteyn, M. M. Murnane, L. Plucinski, D. Steil, B. Stadtmüller, M. Cinchetti, M. Aeschlimann, C. M. Schneider, S. Mathias, Band structure evolution during the ultrafast ferromagnetic-paramagnetic phase transition in cobalt. *Sci. Adv.* **3**, e1602094 (2017).
27. R. Gort, K. Buhlmann, S. Daster, G. Salvatella, N. Hartmann, Y. Zemp, S. Hohenstein, C. Stieger, A. Fognini, T. U. Michlmayr, T. Bahler, A. Vaterlaus, Y. Acremann, early stages of ultrafast spin dynamics in a 3d ferromagnet. *Phys. Rev. Lett.* **121**, 87206 (2018).
28. P. Tengdin, W. You, C. Chen, X. Shi, D. Zusin, Y. Zhang, C. Gentry, A. Blonsky, M. Keller, P. M. Oppeneer, H. C. Kapteyn, Z. Tao, M. M. Murnane, Critical behavior within 20 fs drives the out-of-equilibrium laser-induced magnetic phase transition in nickel. *Sci. Adv.* **4**, eaap9744 (2018).
29. T. Li, A. Patz, L. Mouchliadis, J. Yan, T. A. Lograsso, I. E. Perakis, J. Wang, Femtosecond switching of magnetism via strongly correlated spin-charge quantum excitations. *Nature* **496**, 69–73 (2013).
30. J. K. Dewhurst, P. Elliott, S. Shallcross, E. K. U. Gross, S. Sharma, Laser-induced intersite spin transfer. *Nano Lett.* **18**, 1842–1848 (2018).
31. A. Rundquist, C. G. Durfee, Z. Chang, C. H. NeNe, S. Backus, M. M. Murnane, H. C. Kapteyn, Phase-matched generation of coherent soft X-rays. *Science* **280**, 1412–1415 (1998).
32. C. La-O-Vorakiat, M. Siemens, M. M. Murnane, H. C. Kapteyn, S. Mathias, M. Aeschlimann, P. Grychtol, R. Adam, C. M. Schneider, J. M. Shaw, H. Nembach, T. J. Silva, Ultrafast demagnetization dynamics at the M edges of magnetic elements observed using a tabletop high-harmonic soft x-ray source. *Phys. Rev. Lett.* **103**, 257402 (2009).
33. E. Turgut, C. La-O-Vorakiat, J. M. Shaw, P. Grychtol, H. T. Nembach, D. Rudolf, R. Adam, M. Aeschlimann, C. M. Schneider, T. J. Silva, M. M. Murnane, H. C. Kapteyn, S. Mathias, Controlling the competition between optically induced ultrafast spin-flip scattering and spin transport in magnetic multilayers. *Phys. Rev. Lett.* **110**, 197201 (2013).
34. S. Mathias, C. La-O-Vorakiat, P. Grychtol, P. Granitzka, E. Turgut, J. M. Shaw, R. Adam, H. T. Nembach, M. E. Siemens, S. Eich, C. M. Schneider, T. J. Silva, M. Aeschlimann, M. M. Murnane, H. C. Kapteyn, Probing the timescale of the exchange interaction in a ferromagnetic alloy. *Proc. Natl. Acad. Sci. U.S.A.* **109**, 4792–4797 (2012).
35. M. Hoffner, S. Moretti, J. Shim, S. Häuser, N. Y. Safonova, M. Stiehl, A. Ali, S. Sakshath, J. W. Kim, D. H. Kim, H. J. Kim, J.-I. Hong, H. C. Kapteyn, M. M. Murnane, M. Cinchetti, D. Steil, S. Mathias, B. Stadtmüller, M. Albrecht, D. E. Kim, U. Nowak, M. Aeschlimann, Induced versus intrinsic magnetic moments in ultrafast magnetization dynamics. *Phys. Rev. B* **98**, 174419 (2018).
36. J. K. Dewhurst, K. Krieger, S. Sharma, E. K. U. Gross, An efficient algorithm for time propagation as applied to linearized augmented plane wave method. *Comp. Phys. Commun.* **209**, 92–95 (2016).
37. K. Dewhurst, S. Sharma, C. Ambrosch-Draxl, ELK FP-LAPW Code available at <http://elk.sourceforge.net>.
38. P. Elliott, T. Müller, J. K. Dewhurst, S. Sharma, E. K. U. Gross, Ultrafast laser induced local magnetization dynamics in Heusler compounds. *Sci. Rep.* **6**, 38911 (2016).
39. H. Höchst, D. Rioux, D. Zhao, D. L. Huber, Magnetic linear dichroism effects in reflection spectroscopy: A case study at the Fe M_{2,3} edge. *J. Appl. Phys.* **81**, 7584 (1998).
40. S. Valencia, A. Gaupp, W. Gudat, H.-C. Mertins, P. M. Oppeneer, D. Abramsohn, C. M. Schneider, Faraday rotation spectra at shallow core levels: 3p edges of Fe, Co, and Ni. *New J. Phys.* **8**, 254 (2006).
41. F. Willems, S. Sharma, C. v. K. Schmising, J. K. Dewhurst, L. Salemi, D. Schick, P. Hessian, C. Strüber, W. D. Engel, S. Eisebitt, Magneto-Optical Functions at the 3p resonances of Fe, Co, and Ni: Ab-initio description and experiment. *Phys. Rev. Lett.* **122**, 217202 (2019).
42. P. Grychtol, R. Adam, S. Valencia, S. Cramm, D. E. Bürgler, C. M. Schneider, Resonant magnetic reflectivity in the extreme ultraviolet spectral range: Interlayer-coupled Co/Si/Ni/Fe multilayer system. *Phys. Rev. B* **82**, 54433 (2010).
43. J. L. Erskine, E. A. Stern, Calculation of the M₂₃ magneto-optical absorption spectrum of ferromagnetic nickel. *Phys. Rev. B* **12**, 5016 (1975).
44. A. Eschenlohr, M. Battiato, P. Maldonado, N. Pontius, T. Kachel, K. Holldack, R. Mitzner, A. Fohlisch, P. M. Oppeneer, C. Stamm, Ultrafast spin transport as key to femtosecond demagnetization. *Nat. Mater.* **12**, 332–336 (2013).
45. I. Radu, K. Vahaplar, C. Stamm, T. Kachel, N. Pontius, H. A. Dürr, T. A. Ostler, J. Barker, R. F. L. Evans, R. W. Chantrell, A. Tsukamoto, A. Itoh, A. Kirilyuk, T. Rasing, A. V. Kimel, Transient ferromagnetic-like state mediating ultrafast reversal of antiferromagnetically coupled spins. *Nature* **472**, 205 (2011).
46. D. Rudolf, C. La-O-Vorakiat, M. Battiato, R. Adam, J. M. Shaw, E. Turgut, P. Maldonado, S. Mathias, P. Grychtol, H. T. Nembach, T. J. Silva, M. Aeschlimann, H. C. Kapteyn, M. M. Murnane, C. M. Schneider, P. M. Oppeneer, Ultrafast magnetization enhancement in metallic multilayers driven by superdiffusive spin current. *Nat. Commun.* **3**, 1037 (2012).
47. C. Stamm, T. Kachel, N. Pontius, R. Mitzner, T. Quast, K. Holldack, S. Khan, C. Lupulescu, E. F. Aziz, M. Wietstruk, H. A. Dürr, W. Eberhardt, Femtosecond modification of electron localization and transfer of angular momentum in nickel. *Nat. Mater.* **6**, 740–743 (2007).
48. E. Turgut, D. Zusin, D. Legut, K. Carva, R. Knut, J. M. Shaw, C. Chen, Z. Tao, H. T. Nembach, T. J. Silva, S. Mathias, M. Aeschlimann, P. M. Oppeneer, H. C. Kapteyn, M. M. Murnane, P. Grychtol, Stoner versus Heisenberg: Ultrafast exchange reduction and magnon generation during laser-induced demagnetization. *Phys. Rev. B* **94**, 220408 (2016).
49. Berkeley Center for X-ray Optics: available at <http://www-cxro.lbl.gov>.
50. J. L. Beeby, Electronic Structure of Alloys. *Phys. Rev.* **135**, A130 (1964).
51. E. A. Stern, Rigid-band model of alloys. *Phys. Rev.* **157**, 544 (1967).
52. B. L. Gyorffy, G. M. Stocks, W. M. Temmerman, R. Jordan, D. R. Lloyd, C. M. Quinn, N. V. Richardson, Angle resolved photoemission from a 001 surface of single crystal Ni₂₃Cu₇₇ random substitutional alloy. *Solid State Commun.* **23**, 637–640 (1977).
53. D. Y. Petrovykh, K. N. Altmann, H. Höchst, M. Laubscher, S. Maat, G. J. Mankey, F. J. Himpsel, Spin-dependent band structure, Fermi surface, and carrier lifetime of permalloy. *Appl. Phys. Lett.* **73**, 3459 (1998).
54. J. Minár, S. Mankovsky, O. Šipr, D. Benea, H. Ebert, Correlation effects in fcc-Fe_xNi_{1-x} alloys investigated by means of the KKR-CPA. *J. Phys. Condens. Matter* **26**, 274206 (2014).
55. F. Siegrist, J. A. Gessner, M. Ossiander, C. Denker, Y.-P. Chang, M. C. Schröder, A. Guggenmos, Y. Cui, J. Walowski, U. Martens, J. K. Dewhurst, U. Kleineberg, M. Münzenberg, S. Sharma, M. Schultze, Light-wave dynamic control of magnetism. *Nature* **571**, 240–244 (2019).
56. E. Runge, E. K. U. Gross, Density-functional theory for time-dependent systems. *Phys. Rev. Lett.* **52**, 997 (1984).
57. S. Sharma, J. K. Dewhurst, E. K. U. Gross, Optical response of extended systems using time-dependent density functional theory. *Top. Curr. Chem.* **347**, 235–257 (2014).
58. U. von Barth, L. Hedin, A local exchange-correlation potential for the spin polarized case: I. *J. Phys. C Solid State Phys.* **5**, 1629 (1972).
59. D. J. Singh, L. Nordström, *Planewaves, Pseudopotentials, and the LAPW Method* (Springer, ed. 2, 2006).
60. J. E. Peralta, O. Hod, G. E. Scuseria, Magnetization dynamics from time-dependent noncollinear spin density functional theory calculations. *J. Chem. Theory Comput.* **11**, 3661–3668 (2015).

Acknowledgments

Funding: S.M. and D.S. acknowledge support from the SFB 1073, Project A06. M.A., B.S., B.R., M.H., S.H., and S.T.W. acknowledge support from the SFB/TRR 173 "Spin + X," Project A08. M.M.M. and H.C.K. gratefully acknowledge support for the measurements from the Department of Energy Office of Basic Energy Sciences X-Ray Scattering Program Award DE-SC0002002, a DARPA TEE Award no. D18AC00017, and a Gordon and Betty Moore Foundation EPIQS Award GBMF4538. M.H. and B.S. thankfully acknowledge financial support from the Graduate School of Excellence MAINZ (DFG/GSC 266). S.Sh. would like to thank SFB/TRR 227 "Ultraschnelle Spindynamik" for financial support, and S.Sa. acknowledges financial support from the Carl-Zeiss-Stiftung. **Author contributions:** M.H., T.J.S., H.C.K., B.R., M.C., M.M.M., D.S., B.S., S.Sh., M.A., and S.M. designed the research. M.H., J.K.D., S.H., and S.Sa. performed the research. H.T.N., J.M.S., and T.J.S. contributed new reagents/analytic tools. M.H., P.T., S.T.W., D.S., B.S., and S.M. analyzed the data. M.H., H.C.K., B.R., M.M.M., D.S., B.S., S.Sh., M.A., and S.M. wrote the paper. **Competing interests:** H.C.K. and M.M.M. have a financial interest in KMLabs, which produces the lasers and HHG sources used in this work. H.C.K. is partially

employed by KMLabs. The authors declare that they have no other competing interests. **Data and materials availability:** All data needed to evaluate the conclusions in the paper are present in the paper and/or the Supplementary Materials. Additional data related to this paper may be requested from the authors.

Submitted 30 November 2018

Accepted 9 October 2019

Published 17 January 2020

10.1126/sciadv.aay8717

Citation: M. Hoffherr, S. Häuser, J. K. Dewhurst, P. Tengdin, S. Sakshath, H. T. Nembach, S. T. Weber, J. M. Shaw, T. J. Silva, H. C. Kapteyn, M. Cinchetti, B. Rethfeld, M. M. Murnane, D. Steil, B. Stadtmüller, S. Sharma, M. Aeschlimann, S. Mathias, Ultrafast optically induced spin transfer in ferromagnetic alloys. *Sci. Adv.* **6**, eaay8717 (2020).